Field Crops Research 216 (2018) 175–188

Contents lists available at ScienceDirect

Field Crops Research

journal homepage: www.elsevier.com/locate/fcr

Remote sensing-based crop biomass with water or light-driven crop growth models in wheat commercial fields

Isidro Campos[a,*], Laura González-Gómez[a], Julio Villodre[a], Jose González-Piqueras[a], Andrew E. Suyker[b], Alfonso Calera[a]

[a] GIS and Remote Sensing Group, Instituto de Desarrollo Regional, Universidad de Castilla-La Mancha, Campus Universitario SN, Albacete, Spain
[b] School of Natural Resources, 806 Hardin Hall, University of Nebraska-Lincoln, Lincoln, NE 68583, USA

ABSTRACT

This paper explores the ability of Remote Sensing data from space platforms combined with available meteorological parameters to monitor crop biomass accumulation at satellite scale in a direct, operational way, exploiting the temporal information from time series of multispectral images. We describe a methodology to estimate biomass growth by integrating VI-based biophysical parameter and meteorological input along the growing cycle into the physiologically-based crop growth models, employing water or light use efficiency.

Experimental biomass data of winter and spring wheat (*Triticum aestivum*) growing in commercial plots in Albacete, Spain and Ponca City, OK, USA, under different climates, environment and management, are compared against modeled data. The results exhibit good agreement between measured and modeled biomass data for the calibration and validation datasets. Slopes of the linear relationships provide empirical values of the efficiencies of the whole process of biomass production: light use efficiency (LUE), water use efficiency (WUE) and normalized water productivity (WP*). These values are comparable to the experimental values published in the literature.

1. Introduction

The estimation of biomass production has a prominent role in the strategies to increase crop productivity and improve management efficiency. Monitoring biomass production is a diagnostic tool for the evaluation of crop management because the accumulation of biomass responds to the coupled effects of climate (Fischer, 1993; Garcia et al., 1988; Raes et al., 2008) crop genomics (Calderini et al., 1997; Siddique et al., 1990), and nutrient/water management (Fischer, 1993; Green, 1987; Latiri-souki et al., 1998). The simulation of biomass production during the growing cycle has interesting application for the assessment of the fertilization necessities, essential in the strategies of nitrogen variable doses in coordination with the diagnosis tools for remote estimation of nitrogen concentration (Fitzgerald et al., 2006; Houlès et al., 2007). In addition, biomass accumulation is strongly related to yield production in grain crops although not in an unequivocal way (Aase and Siddoway, 1981; Padilla et al., 2012). The crop yield can be estimated as a variable proportion of total aboveground biomass that goes into the harvestable parts depending on biotic and abiotic stresses, the duration, the severity and the physiological stage of the crop during the stress period (Fischer and Maurer 1978). This proportion is known as harvest index (HI).

The classical approach to the simulation of biomass production is the use of a crop growth model (CGM) based on either light or water use efficiency. This approach relies on the quantitative knowledge of the parameters describing the canopy interaction with solar radiation and the exchange of water transpired by the canopy (Hoogenboom 2000). Simulation of leaf area development is the usual key parameter for the estimation of fraction of incident PAR that is absorbed by the canopy (fAPAR) for those CGMs based on Light Use Efficiency (LUE). This is essentially the background of STICS (Brisson et al., 1998), EPIC (Williams et al., 1990) and CERES (Jones and Kiniry, 1986) as the crop growth module in HybridMAIZE and DSSAT (Jones et al., 2003). The models based on the Water Use Efficiency (WUE) such as AquaCrop (Steduto et al., 2009) or a hybrid approach like CropSyst (Stockle et al., 1994) simulate canopy cover development for the estimation of a transpiration coefficient (K_t), or basal crop coefficient. The ongoing discussion of the WUE dependence on climate has led to the development of normalized WUE by using reference ETo, introducing normalized Water Productivity (WP*). The simulations of the key biophysical parameter in each model must be adapted for each crop, environmental conditions and management.

For an operation description of crop biophysical parameters, remote

* Corresponding author.
E-mail address: campos.isidro@gmail.com (I. Campos).

https://doi.org/10.1016/j.fcr.2017.11.025
Received 6 July 2017; Received in revised form 24 November 2017; Accepted 25 November 2017
Available online 28 November 2017
0378-4290/

sensing (RS) measurements can provide temporal information on plant responses to dynamic weather conditions and management practices. Thus, RS approaches exhibit a large potential to provide biomass and final yield assessments in addition to variations across fields (Pinter et al., 2003). In the framework of yield/biomass estimates, the use of RS data has followed three main approaches (Sadras et al., 2015): integration/assimilation of RS derived variables into CGM, direct reflectance-based empirical relationships on selected dates, and biomass accumulation models. Empirical relationships have interesting applications for regional yield estimates (Lobell et al., 2003) and yield prediction (Sibley et al., 2014). However, these relationships must be locally calibrated, considering the uncertainties related with the selection of the most representative date for the assessment of biomass production and spatial variability.

The assimilation of RS data has been frequently proposed in the scientific literature in order to initialize, calibrate, or update CGMs (Clevers et al., 1994). On this line Bouman (1992) and Clevers et al. (1994) proposed the initialization (showing date) and re-parametrization (canopy expansion parameters) of the SUCROS model based on radar and canopy reflectance information in sugar beet. Sibley et al. (2014) assimilates RS-based fPAR estimates into the Hybrid-Maize model varying the sowing date, seeding density, and maturity rating of the hybrids (measured as thermal accumulation needed for the crop to reach physiological maturity). Trombetta et al. (2016) proposed the modification of the parameters describing the crop phenology and expansion into AQUACROP based on a relationship between ground cover and leaf area index (LAI) derived from RS data. Jin et al. (2017a,b) assimilated ground cover estimates based on optical and radar into the AQUACROP model. After assimilation, the model is calibrated in terms of canopy expansion and evaluated for the assessment of grain production at regional scale. The calibration of the initial conditions in assimilation methods can be limited by the availability on input data, since the number of parameters to be calibrated depend on the variables actually available. In a simpler approach, Padilla et al. (2012) assimilated RS-based LAI values into the GRAMI model, avoiding the calculation of the most complex processes such as water stress, nitrogen nutrition or plant population density. In the same line, the most recent versions of AQUACROP allows to incorporate canopy cover measurements for a better representation of the crop characteristics. These later assimilation/integration methods suppose a great simplification, but still rely on the aptitudes of the models to reproduce the key variables (PAR absorption or crop transpiration) from related biophysical parameters such as LAI or ground cover.

In this work, we specifically focus on the capability of temporal series of multispectral images combined with available meteorological data to provide, along the entire growing cycle, the key variables into the engine of the models based on LUE and WUE for the estimation of biomass accumulation. We are following the line proposed by Daughtry et al. (1992) working in corn and soybean with models based on LUE, but we are extending this approach to the models based on water use and providing new evidences in a different crop (wheat), monitored in field conditions, and at the scale of commercial farm. This direct approach provides a physically-based agronomic monitoring systems (Daughtry et al., 1992) but it has been hardly explored in the scientific literature. Special mention deserve the work done by Bastiaanssen and Ali, (2003), Zheng et al. (2016) and Zwart and Bastiaanssen, (2007) proposing the integration of RS-based fPAR for the assessment of yield at regional and global scales and some recent experiments (Campos et al., 2017b) demonstrating the feasibility of RS-based K_t for the assessment of biomass and yield in corn and soybeans. Nevertheless, the literature is scarce in comparative studies, analyzing the aptitudes of the models based on water and light use for a common database.

In contrast with previous research, we compared three different approaches for the assessment of biomass, from the most common LUE models to the WUE and WP* approaches. The novelty is the analysis of light use efficiency and water use efficiency approaches using a common base for the estimation of the key variables, fPAR and K_t, and the analysis of the precision of the models under different conditions. The thorough selection of experimental datasets allows us to evaluate and discuss, with empirical evidences, the feasibility of these approaches for wheat under different climatic, management and deficit conditions. The specific objectives are: i) the estimation of the parameters LUE, WUE and WP* for wheat based on the proposed approach; ii) the evaluation of the three models under field conditions and considering the possible effect of nitrogen deficit and climatic conditions. In addition, this paper provides a comprehensive explanation about the foundations of the use of RS data in CGMs and the benefits and constrains of this direct method. Considering that the proposed method represents a considerable simplification with respect to previous approaches, we analyzed and discussed with respect to previous research the model parametrization (LUE, WUE and WP* values) and the exactitude of the models to estimate biomass production.

2. Materials and methodology

2.1. Basis of growth models

Vegetation growth and biomass accumulation occur as consequence of CO2 assimilation and water transpiration flux through plant stomas during the photosynthesis process, in which the required energy is provided by solar radiation (Rosenberg et al., 1983). Attending to the physiological basis of the process, the classical approaches for growth simulation are based in the efficiency of the conversion of the water transpired or the light absorbed into biomass. These two classical models are known as water use efficiency and light (or radiation) use efficiency approaches and both approaches represent the core feature of the "growth-engine" of many crop models (Steduto and Albrizio, 2005).

2.1.1. Biomass production based on radiation/light use efficiency model

Radiation use efficiency was formulated by Monteith (1972) and it focuses on the relationship between the rate on the dry biomass gain (Biomass) and the absorbed solar radiation by the leaves in the wavelengths of the incident photosynthetically active solar radiation (PAR). Thus, the relationship is stablished in terms of the PAR absorbed by the leaves and used in the photosynthesis process (Eq. (1)).

$$Biomass = \int_{t_o}^{t} LUE \cdot APARd(t) \quad (1)$$

where Biomass is the dry biomass per unit of surface gain during the period between t_0 and t in g m^{-2}; LUE is the light use (photochemical) efficiency factor in g MJ^{-1}; APAR, is the PAR absorbed in MJ/m2, represents the photon flux absorbed by the canopy photosynthetic elements.

2.1.2. Biomass production based on water use efficiency models

The models based on the water use efficiency are probably the initial approaches to crop-growth, based on the quantitative statements settled by some pioneers like Briggs and Shantz (1913). These models estimate the rate of Biomass as the integral over the time of the product of crop transpiration multiplied by the term water use efficiency (WUE). Considering that the effect of water stress could reduce the crop transpiration, the relation is stablished in terms of adjusted crop transpiration accounting for water stress conditions ($T_{c,adj}$) as presented in Eq. (2).

$$Biomass = \int_{t_o}^{t} WUE \cdot T_{c,adj} d(t) \quad (2)$$

where $T_{c,adj}$, crop transpiration accounting for water stress conditions in mm; WUE, water use efficiency in g m^{-2} mm^{-1}, is the slope of the relationship between Biomass accumulation and $T_{c,adj}$.

2.1.3. Biomass production based on normalized water productivity models WP*

In spite of the general agreement about the essentially constant (or linear) relationship between biomass and $T_{c,adj}$, the effect of climatic conditions on these relationships is also recognized. Essentially the literature distinguishes between the normalization of WUE using vapor pressure deficit (VPD) or ETo. This discussion was reanalyzed in great depth by Steduto and Albrizio (2005) and Steduto et al. (2007) concluding the ETo as the best climate normalization for WUE and introducing the concept of normalized water use efficiency (WP*). The relationship between Biomass and the cumulative value of the ratio between $T_{c,adj}$ over ETo is presented in the Eq. (3). This is the methodology followed in the AQUACROP model and popularized in the FAO-66 manual (Steduto et al., 2012).

$$Biomass = \int_{t_o}^{t} WP^{*}\cdot K_{st}\cdot \frac{T_{adj}}{ETo} d(t) = \int_{t_o}^{t} WP^{*}\cdot K_{st}\cdot K_{t,adj}\, d(t) \quad (3)$$

where $K_{t,adj}$ is the crop transpiration coefficient accounting for water stress conditions, K_{st} is the temperature stress coefficient and WP* is the normalized water productivity, in g m^{-2}.

The formulation presented in the Eqs. (1), (2) and (3) assumes that the efficiencies (LUE, WUE and WP*) are dynamic and could change during the growing cycle because of factors related with the meteorological conditions and the crop physiology and management. These factors must be considered but assuming constant values suppose an operational advantage for the estimation of Biomass production. In this case, the numerical integration of either APAR, either $T_{c,adj}$ or $K_{t,adj}$ provides biomass accumulation estimates.

PAR absorption is generally approximated by the fraction of PAR intercepted by the whole canopy (IPAR), assuming that the radiation interception by non-photosynthetic elements is low (Asrar et al., 1984). Hence the value of IPAR can be estimated by the product: fPAR*PAR_{in}. fPAR is the fraction of PAR_{in} intercepted by the vegetation. The value of $K_{t,adj}$ can be estimated by the product of transpiration coefficient (K_t) and the crop water stress coefficient (K_{sw}). The coefficient K_t is the ratio of crop transpiration to atmospheric demand under non-limiting moisture conditions; equivalent to the basal crop coefficient, K_{cb}, defined by Allen et al. (1998) but different in terms of the minimum K_t equal to 0 for bare soil conditions. The coefficient K_{sw} is the ratio of actual crop transpiration to crop transpiration under non-limiting moisture conditions (T_c). By the same definition the value of $T_{c,adj}$ can be estimated by the product K_t*K_{sw}*ETo.

2.2. Integrating remote sensing into the basis of growth models

As described in the previous section, a key point for the models based on LUE and water use efficiency is the determination of APAR and $T_{c,adj}$, which strongly depend on the parameters fPAR and K_t respectively. These models also depend on the stress coefficients already mentioned and described in the Section 2.4. The continuous measurement across space and time of fPAR, and K_t parameters is usually difficult and only possible in few well controlled experiments. Nevertheless, time series of remote sensing data offers a unique way to monitor fPAR, and K_t during the whole growing season. The estimation of fPAR and K_t from RS includes empirical relationships with spectral vegetation indices (VI) and the inversion of analytical models like radiative transfer and spectral mixture analysis approaches. We centered the analysis using the relationships of fPAR and K_t with VI. Nevertheless, we contemplate that other approaches could be more suitable to retrieve the needed biophysical parameters for determinate canopies or scales. Thus the methodology proposed in this paper does not depend on the method followed and is compatible with other approaches to compute K_t or fPAR.

2.2.1. Remote sensing of fPAR

The satellite-reflectance based VI is a measurement of canopy light absorption rather than a surrogate for detailed features of canopy architecture (Glenn et al., 2008). The link between fPAR and spectral VI is well-documented and recurrently presented in the literature by empirical and analytical studies (Calera et al., 2004; Baret and Guyot, 1991; Daughtry et al., 1992; Sellers, 1985). The relationship was demonstrated linear if the soil or background material underlying the canopy is relatively dark (Asrar et al., 1984; Sellers et al., 1992). Lobell et al. (2003) proposed the estimation of fPAR rescaling the VI between the minimum values of VI and fPAR for the analyzed canopy, bare soil conditions, and the maximum values of VI and fPAR. This relationship (Eq. (4)) accounts for the site to site variations of the minimum VI and the possible saturation of fPAR before the VI reach its maximum value.

$$fPAR = \frac{(VI - VI_{min})\cdot(fPAR_{max} - fPAR_{min})}{(VI_{max} - VI_{min})} + fPAR_{min} \quad (4)$$

where VI is the actual value of the analyzed VI, VI_{min} is the minimum value of VI corresponding to the minimum value of fPAR ($fPAR_{min}$) and VI_{max} is the value of the analyzed VI corresponding to the maximum fPAR ($fPAR_{max}$) reached by this canopy during the crop growth.

In this work, we used the relationship between fPAR and the normalized difference vegetation index (NDVI) published by Asrar et al. (1984) for wheat, see Eq. (5). The Eq. (5) is similar to the empirical regression obtained by Daughtry et al. (1992) in wheat (fPAR = 1.25·NDVI-0.21) and it is equivalent to Eq. (4) based on the NDVI and for $NDVI_{min}$ = 0.15, $NDVI_{max}$ = 0.91, $fPAR_{min}$ = 0.001 and $fPAR_{max}$ = 0.95. These values are withing the ranges of minimum NDVI determined by Asrar et al. (1984) under base soil conditions, NDVI = (0.10–0.20) for LAI = 0, and the NDVI determined by these authors for wheat at full cover, NDVI around 0.9 for LAI > 3. In addition, this parametrization coincides with the ranges of fPAR considered in previous studies in wheat (Zheng et al., 2016; Daughtry et al., 1992) and the maximum value of NDVI is similar to other maximum values reported for wheat (Duchemin et al., 2006). The value of $NDVI_{min}$ is similar to the values obtained in our study for bare soil in the Spanish study area, and is slightly lower than the minimum values measured in Ponca (0.18). The use of both minimum values (0.15 or 0.18) results in a difference lower than the 5% of the average fPAR estimated during the whole growing cycle for the analyzed dataset. Consequently, we used the equation proposed by Asrar et al. (1984) in this work and further adaptations can be specifically developed for other areas.

$$fPAR = NDVI\cdot 1.25 - 0.19 \quad (5)$$

2.2.2. Remote sensing of transpiration coefficient

The estimation of the transpiration coefficient obtained from spectral VI has been widely evaluated for multiple crops (Glenn et al., 2011). The relationship between K_t and VI used in this work is based on the method proposed by Choudhury et al. (1994) and modified by González-Dugo and Mateos (2008). These authors proposed a potential approach rescaling the VI values between the minimum VI values in the area (bare soil conditions) and the VI coinciding with the saturation of the K_t. This relationship (Eq. (6)) accounts for the site to site variations of the minimum VI. The minimum K_t is assumed equal to 0 in this formulation.

$$K_t = K_{t,max}\cdot\left[1 - \left(\frac{(VI_{max} - VI)}{(VI_{max} - VI_{min})}\right)^{\alpha}\right] \quad (6)$$

where VI is the actual value of the analyzed VI, VI_{min} is the minimum value of VI corresponding to bare soil conditions, VI_{max} is the value of the analyzed VI corresponding to the maximum K_t ($K_{t,max}$) reached by this canopy and α is the exponent of the relationship.

In this work, we used the relationship K_t-NDVI published by Duchemin et al. (2006) for wheat, see Eq. (7). The Eq. (7) is equivalent

to Eq. (6) based on the NDVI and for $NDVI_{min}$ = 0.14, $NDVI_{max}$ = 0.91, $K_{t,max}$ = 1.26 and α = 1 (linear relationship). The range of NDVI mostly agree with the NDVI values already discussed for wheat in the study areas. The maximum K_t slightly greater than maximum values recommended in the FAO-66 (Steduto et al., 2012) and FAO-56 manuals (Allen et al., 1998) but this limit coincides with the experimental values of the transpiration coefficients measured empirically in wheat (Choudhury et al., 1994; Duchemin et al., 2006). Addition uncertainties for the used equation is the saturation effect expected for the relationship between LAI and NDVI. It is generally accepted that the NDVI saturates for LAI around 3 for many canopies (Campos et al., 2017c; Neale et al., 1989). For wheat, this saturation limit (LAI = 4) coincides with the saturation of the relationship between K_t and LAI and consequently, the relationship between NDVI and K_t can be considered linear (Duchemin et al., 2006). Further relationships between the transpiration coefficient and the most recent vegetation indices have been developed (Marshall et al., 2016) providing promising results. However, the use of the most basic multispectral indices have been demonstrated valid for the assessment of K_t in multiple canopies (Bausch and Neale, 1987; Campos et al., 2016; Er-Raki et al., 2007; Hunsaker et al., 2003; Odi-Lara et al., 2016) and ensures the possibility to use multiple platforms for the assessment of biomass production as reasoned in the discussion section.

$$K_t = 1.64 \cdot (NDVI - 0.14) \quad (7)$$

2.3. Operational estimation of biomass based on the proposed approaches

These previous evidences let us to introduce the formalism of the relationship between crop biomass production and the accumulated value of the reflectance based VIs. But this relationship is modulated by the atmospheric conditions represented by PAR, ETo or K_{st} (based on air temperature) as highlighted by Hoogenboom (2000). In addition, the efficiencies (LUE, WUE and WP*) are generally considered dynamic, being affected by temperature (high and low) and nutrition (fertilization) stresses. The stresses considered in this work and the calculation procedures are presented in the next section.

The estimation of the biophysical parameters used in each model (see Fig. 1a) was based in the daily interpolated values of NDVI and the relationships presented in Eqs. (5) and (7). The method to solve the integrals presented in Eqs. (1)–(3) is to calculate Biomass by numerical integration of the dependence function using data in adequate temporal resolution. The best time scale to simulate the crop biomass production is daily (Steduto et al., 2012), prompting the necessity of daily values of the biophysical parameters K_t and fPAR. The meteorological data required are usually available at daily scale. Thus K_t and fPAR or simply the used VI must be interpolated from the time-discrete data derived from RS data. The NDVI describe a smooth-continuous function over the time when plotted versus the time measured as days, GDD or accumulated ETo (see Fig. 1a). The high frequency of satellite images obtained in this study, with around 2–3 images per month, for most of the analyzed fields, allows for an adequate description of the wheat development and the daily data can be easily obtained using a linear interpolation between the available data (see Fig. 1a).

The daily values of the biophysical parameters so obtained are multiplied by the corresponding meteorological variable, ETo and incident PAR and the daily water stress coefficient in order to compute the daily values of the variables $T_{c,adj}$, IPAR or $K_{t,adj}$*K_{st}. (see Fig. 1b). The accumulated value of this variables is compared with the crop Biomass (see Fig. 1c) through linear regression. The slope of this correlation coincides with LUE, WUE or WP* and the interception is ideally around 0. Although experimental values of LUE, WUE and WP* are regularly published, the strong variability of LUE and WUE values and scarcity of WP* data let us to develop of empirical values that will be evaluated for the validation datasets and discussed with respect to the values founded in the literature. In this work we initially evaluated the use of constant values of LUE, WUE or WP* and the necessity to consider dynamic values for each efficiency is discussed in view of the results.

Biomass estimation is based on a definite integral for which the dates for T_0 and T must be known. In this study, the selection of the date for the beginning of the biomass accumulation was based on the detection of the green-up phase. The green-up represents the earliest time that vegetation growth can be reliably detected by satellite and coincides with the inflexion of the curve fitting the temporal evolution of the NDVI. This inflexion occurred for NDVI values between 0.2 and 0.3 in the analyzed fields (see Fig. 1a) in agreement with the results obtained by (Lobell et al., 2013) for winter wheat growing in India. The green up does not coincides with the beginning of the biomass accumulation (emergence), but the uncertainty selecting this point with respect to the emergence date was estimated in less than 50 g m^{-2}. Conversely, the final of the biomass accumulation occurs before the inflexion describing the senescence of the wheat canopy. According with our experience in the direct observation of wheat phenology, the

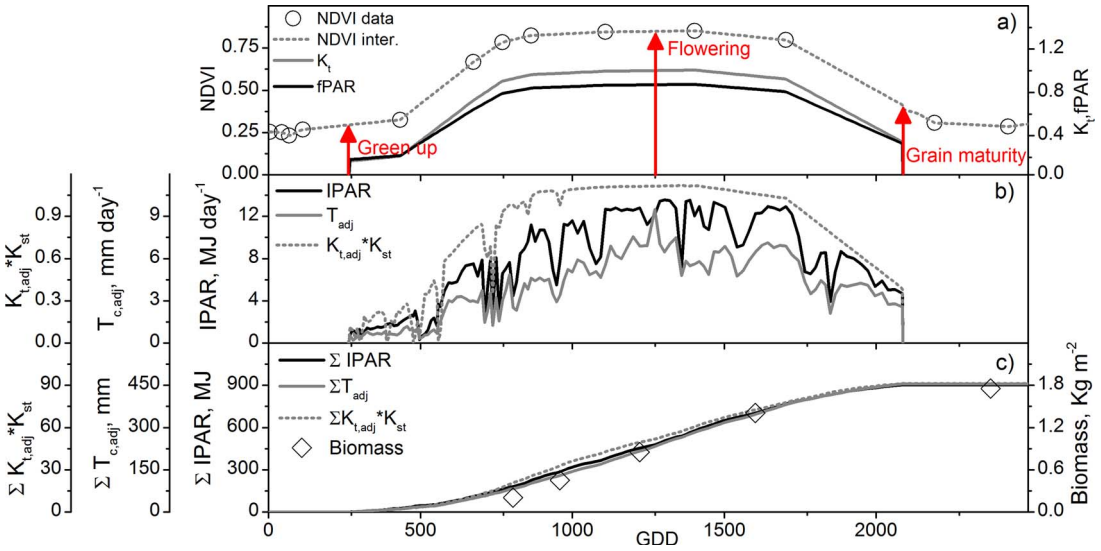

Fig. 1. a) example of the temporal evolution on the measured NDVI, interpolated values of NDVI, daily values of the fraction of PAR intercepted (fPAR) and transpiration coefficient (K_t) for the Field 1. b) temporal evolution of the PAR intercepted (IPAR), crop transpiration including water stress ($T_{c,adj}$) and the product of the crop transpiration coefficient including water stress.

Table 1
Coordinates, irrigation and fertilization doses in the calibration and validation sites.

Fied ID	Year monitored	Managemet	Variety	Irrigation mm	Fertilization, Kg (N, P, K)	Yield (t/ha)	Coordinates
1	2015	Irrigated, direct seeding	Califa	452	(257, 81; 65) 5 doses	9.22	39.25° N, 1.99° W
2	2016	Irrigated, conventional	Califa	580	(294, 129; 55) 5 doses	9.41	39.13° N, 2.91° W
3	2016	Irrigated, conventional	Califa	461	(349, 132; 165), 6 doses	10.10	38.89° N, 1.87° W
4	2015	Irrigated, direct seeding	Galera	230	(140, 79; 0), 3 doses	3.84	39.08° N, 1.66° W
5	2015	Irrigated, conventional	Califa	447	(268, 120; 150), 6 doses	7.06	38.87° N, 1.84° W
6	98–99	Rainfed, conventional	AsegCo 2174	–	(88; 26; 0), 1 dose	NA	36.77° N, 97.15° W
6	99–00	Rainfed, conventional	AsegCo 2174	–	(88; 26; 0), 1 dose	NA	36.77° N, 97.15° W

physiological maturity of the grain occurs for NDVI values around 0.4 for irrigated wheat. This empirical evidence is based in few experiments (20 commercial fields monitored during 10 growing seasons) and could vary for the different varieties and managements, but was used in this study in order to delimit the definite integral used for the delimitation of the growing cycle. For additional information about the estimation of the maturity stage, the reader is referred to González et al. (2017).

2.4. Estimation of abiotic stress

The abiotic stresses considered in this work were the crop water stress (K_{sw}), the cold temperature stress coefficient (K_{st}) and the nitrogen stress characterized by the Nitrogen Nutrition Index (NNI). Both WP* and WUE are insensitive to crop water stress, already included in the variable $T_{c,adj}$, but this factor could affect LUE for wheat and consequently the effect of the water stress was included in the LUE formulation by multiplying the estimates of IPAR times K_{sw} at daily scale. Thermal (cold) stress affects biomass production in wheat and is already included in the formulation based on WP* by introducing the coefficient K_{st}. The effect of cold stress in WUE and LUE models is not questionable, but at the first approach we did not include the coefficient K_{st} into the LUE and WUE models, the convenience of the inclusion of this coefficient in the noted models is analyzed in the discussion section. Finally, the literature is not conclusive about the effect of nitrogen deficit because this factor reduces essentially the plant development but not necessarily the efficiency of the actual canopy in producing biomass. This point was analyzed in this study since the validation dataset includes experimental data of wheat biomass production under nitrogen deficit.

The K_{sw} was computed for every field following the soil water balance model described in the FAO-56 manual and assimilating the basal crop coefficient derived from satellite images. The lack of knowledge with regard the soil properties prevents the use of more complex approaches as is the case of FAO-66. Even considering the relative simplicity of the FAO-56 approach, the absolute values and the spatial distribution of those parameters which define the soil water available for the plants, are subjected to a great uncertainty in commercial fields.

The remote sensing based soil water balance model used in this work was already discussed in Campos et al. (2017c), Campos et al. (2016) and Gonzalez-Dugo et al. (2009). The model was applied in a diagnostic mode, so the meteorological data and actual irrigation data were assimilated in the model and the water stress, K_{sw}, was simulated. For further information about the model, the reader is referred to the previous references. The main difference with respect to previous approaches in the parametrization in terms of root depth and soil properties. The temporal evolution of K_{sw} analyzed in this work is the average of the K_{sw} obtained from 10 simulations of the soil water balance considering a maximum root depth of 100 cm in the American study area (Allen et al., 1998) and 60 cm in the Spanish study area, due to the limitations in soil depth. The range of available water considered in the simulations varies from 100 to 150 mm m^{-1}. The temporal evolution of K_{st} was estimated following the logistic function and the extremes for the biomass production (0 and 13 °C) as described by Raes et al. (2011). The NNI was computed as the difference between N_{act} and the critical nitrogen concentration (N_c) (Angus and Moncur, 1985; Greenwood et al., 1986). The values of N_c and were derived from the critical dilution curves proposed by Justes et al. (1997) for wheat.

2.5. Study sites and ground measurements: total aboveground biomass, ETo and PAR data

The field data analyzed in this work was divided into calibration and validation datasets. The calibration dataset was obtained in three fields located in Albacete (South-East of Spain). These fields (Field 1, 2 and 3) were monitored in 2015 and 2016 during the spring wheat growing cycle, from January to July. The validation dataset was comprised of three fields (fields 4, 5 and 6). Fields 4 and 5 was located in Albacete and was monitored in 2015 during the spring wheat growing cycle. Field 6 is located in Ponca City, OK (north-central Oklahoma, USA) and was monitored during the winter wheat growing cycles in 1998–1999 and 1999–2000 (AmeriFlux site designation: US-Pon). The coordinates of each field are presented in Table 1. The climatology in the Spanish study area is Mediterranean. The mean annual precipitation for the last thirty years was 340 mm and the mean annual temperature was 13.6 °C for the same period. The climate in Ponca City is Continental sub-humid, the mean annual temperature for years 1961–1990 was 15.03 °C with a range of −3.7–33.9 °C. The annual average precipitation for the same period was 835 mm.

Fields 1–5 are commercial fields planted with spring wheat varieties and irrigated with center pivot systems. Field 1 and Field 4 are managed under minimum tillage and direct seeding. Fields 2, 3 and 5 were managed following traditional tillage and showing practices and the management of the Field 5 included the incorporation of the rest of the previous crop (corn). The irrigation timing varies from weekly events at the beginning of the season in January to daily applications during May. Fertilizer was applied in split portions at different growth stages. Irrigation and fertilization totals and the number of applications for every field are presented in Table 1. Field 6 is a rained commercial field and was managed following the traditional tillage/fertilizing practices in this region. Even though the field was under rainfed conditions, crop water availability was adequate during most of the growing cycle (Burba and Verma 2005).

The samples of aboveground biomass were collected at 6–9 measurement locations per field at a minimum of 5 dates during the growing cycle in the fields 1–5. Each sample is composed by 3 subsamples where the aboveground biomass present in 2 rows along 1.5 m was collected manually and dried for 48 h at 60 °C. The same samples were used to determine the nitrogen concentration (%) at the plant level (N_{act}). Each of the measurement locations is in a homogeneous zone with a minimum area of 1 ha (see Fig. 2). The homogeneous areas were delimited based on the cumulated values of NDVI interpolated at daily scale during two to three previous campaigns (Campos et al., 2014). This method assumes that the presence or areas with differential crop development during two or more growing seasons denotes differences in the soil structure and similar differences can be expected during the current growing season. The samples of aboveground biomass in the field 6 were collected at four locations, with 0.5 m of a row sampled in each area. Experimental measurements of N content were

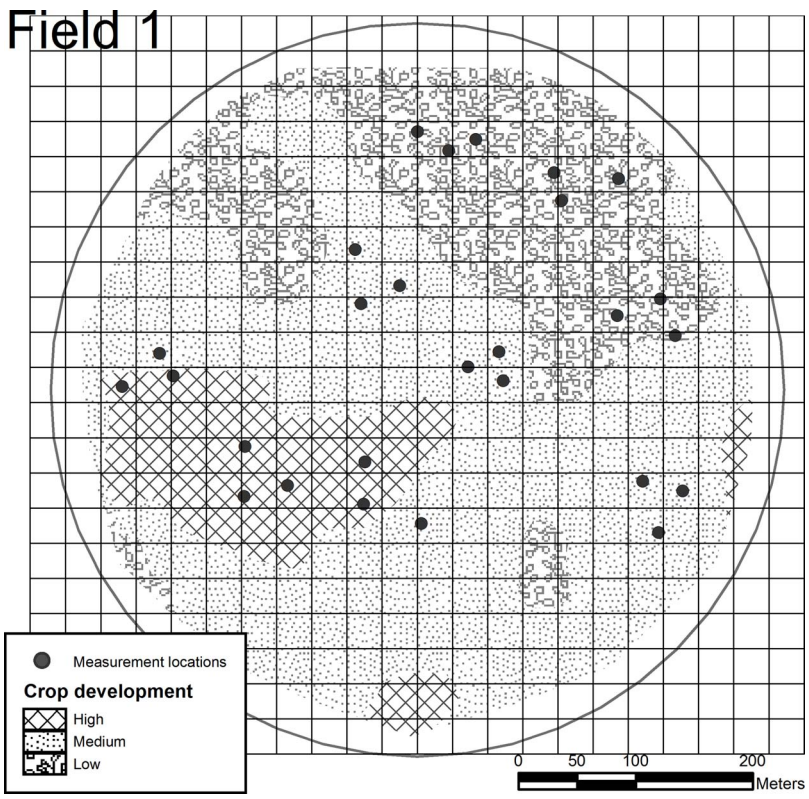

Fig. 2. Example of the homogeneous areas, measurement locations and pixel size (30 m) in the field 1.

not available for the field 6 (Fig. 2).

Considering the objectives of this analysis, the validation and calibration datasets were in sharp contrast with respect to location, varieties, stresses, management practices and climate. No nitrogen or water deficit was detected in the field 1, 2 and 3 while the field 4 and 5 were under water and/or nitrogen deficits as presented in the results section. Field 6 was winter wheat planted in a different climatic conditions, and these factors guarantee the differences in those variable related with the meteorological conditions during the growing cycle.

Meteorological data used in this study include maximum and minimum daily temperature, incoming solar radiation (R_s), maximum and minimum daily relative humidity and wind speed. These data were used to compute a) the daily reference evapotranspiration (ETo) following the FAO-56 formulation for grass reference (Allen et al., 1998), b) growing degree days (GDD) with base temperature of 0 °C and a maximum temperature of 25 °C (McMaster and Smika, 1988), c) daily incident photosynthetically active radiation (PAR) as the half part of R_s (Campbell and Norman, 1998). These data were downloaded from the meteorological services SIAR (Servicio Integral de Asesoramiento al Regante, http://crea.uclm.es/siar/) in Spain and Oklahoma MESONET (Oklahoma MESOscale NETwork, https://www.mesonet.org/) in USA. The nearby stations to the study field were selected (station La Gineta in Spain and Blackwell in USA).

2.6. Remote sensing data

The analyses of the experimental data performed in this work, length of the growing cycle and biophysical parameters, were based on NDVI data derived from satellite images. The reflectance data used to compute the NDVI were obtained from Landsat 8 and 7 in the fields 1 to field 5 during the years 2015–2016. The reflectance data analyzed for the field 6 were obtained from Landsat 5 and Landsat 7 images, the images acquisition dates are presented in Table 2. Unfortunately no images were available for the field 6 at the beginning of the growing season. Thus, an initial value of NDVI equal to 0.18 was assumed on November 15th 1998, based on the temporal evolution of the LAI data and the NDVI values for bare soil in the study area. The satellite images are atmospherically corrected. Considering the possible difference between the maximum NDVI derived from Landsat 8 and Landsat 7 with respect to Landsat 5, we applied a normalization procedure based on pseudo-invariant surfaces (dense vegetation like alfalfa and agricultural bare soils) and every image were rescaled to the NDVI range obtained for Landsat 5.

The Landsat collection terrain corrected product (Level-1 TP) provides a geometric precision greater than 0.5 pixels (12 m) for the 90% of the analyzed area. The method selected for the compensation of the atmospheric distortion was based on the selection of pseudo-invariant surfaces (dense vegetation and agricultural bare soil) following the methodology described by Chen et al. (2005). The data obtained in this work was based exclusively in Landsat images (Landsat 5, 7 and 8) because of the availability of operations medium resolution sensors during the analyzed periods. The study fields was monitored during the years 1998–2000 and 2015, with low availability of operational satellite. During the last analyzed campaign, the images available was Landsat 7 and 8 in addition to the recent Sentinel 2-A. The time series derived exclusively from Landsat constellation was sufficient to describe the temporal evolution of the analyzed fields.

The temporal evolutions of the needed parameters (fPAR or Kt) were estimated for 3 by 3 pixels (90 by 90 m) centered in the measurement locations. The analyses performed in this work, the correlation versus the measured biomass and the evaluation of the model precision, are based on the average value. In addition, the variability in each measurement location was analyzed in terms of the standard deviation (SD) of the accumulated value of the NDVI during the growing cycle in each group of 9 pixels.

3. Results

3.1. Field data analysis: crop development and meteorological conditions

3.1.1. Calibration dataset

The temporal evolution of the NDVI describe similar and typical

Table 2
Acquisition dates of the images and field measurements of canopy reflectance used in the study.

Field 1	Field 2	Field 3	Field 4	Field 5	Field 6 98–99	Field 6 99-00
Jan. 5, 2015	Jan. 8, 2016	Jan. 8, 2016	Jan. 5, 2015	Jan. 5, 2015	Jan. 4, 1999	Oct. 27, 1999
Jan. 14, 2015	Jan. 17, 2016	Jan. 17, 2016	Jan. 14, 2015	Jan. 14, 2015	Jan. 20, 1999	Nov. 12, 1999
Mar. 10, 2015	Jan. 24, 2016	Jan. 24, 2016	Mar. 10, 2015	Jan. 30, 2015	Mar. 9, 1999	Nov. 20, 1999
Apr. 3, 2015	Feb. 2, 2016	Feb. 2, 2016	Apr. 3, 2015	Mar. 10, 2015	May. 12, 1999	Nov. 28, 1999
Apr. 12, 2015	Mar. 5, 2016	Mar. 5, 2016	Apr. 20, 2015	Apr. 3, 2015	May. 28, 1999	Dec. 6, 1999
Apr. 20, 2015	Mar. 12, 2016	Mar. 12, 2016	May 6, 2015	Apr. 12, 2015	Jul. 15, 1999	Dec. 30, 1999
May 6, 2015	Mar. 29, 2016	Apr. 6, 2016	May 21, 2015	May 6, 2015	Jul. 23, 1999	Jan. 7, 2000
May 22, 2015	May 24, 2016	May 24, 2016	May 22, 2015	May 13, 2015		Feb. 8, 2000
Jun. 7, 2015	Jun. 9, 2016	May 31, 2016	May 30, 2015	May 21, 2015		Mar. 27, 2000
Jun. 30, 2015	Jun. 16, 2016	Jun. 9, 2016	Jun. 7, 2015	May 22, 2015		Apr. 4, 2000
Jul. 9, 2015	Jul. 2, 2016	Jun. 13, 2016	Jun. 22, 2015	May 30, 2015		May 30, 2000
Jul. 16, 2015		Jun. 25, 2016	Jun. 30, 2015	Jun. 7, 2015		Jun. 7, 2000
		Jul. 2, 2016	Jul. 9, 2015	Jun. 22, 2015		Jun. 15, 2000
		Jul. 11, 2016	Jul. 16, 2015	Jun. 23, 2015		Jun. 23, 2000
				Jun. 30, 2015		Jul. 1, 2000
				Jul. 9, 2015		
				Jul. 16, 2015		

Table 3
Length of the growing cycles estimated from green-up to maturity.

	Field 1	Field 2	Field 3	Field 4	Field 5	Field 6 98–99	Field 6 99-00
Days	168	175	142	115	110	223	205
GDD, °C	1993	2047	1805	1490	1576	2360	2160
Mean T[a], °C	11.9	11.7	12.7	13.2	14.3	11.3	16.9
ETo, mm	606	602	558	453	470	620	560

pattern for every field in the calibration dataset, with a rapid growth after the emergence (January-February) followed by a plateau during 4–8 weeks. The senescence was also fast coinciding around the beginning of June for every analyzed field and the differences in planting dates also impose differences in the senescence. The lengths of the growing cycles measured in days, GDD and accumulated ETo are presented in Table 3. Although all three fields are subjected to similar climatological conditions, the inter-annual variations and the differences in the length of the growing cycle result in notable differences in terms of accumulated ETo during the cycle. The maximum NDVI values were registered in the middle of the plateau, being the maximum values around 0.85 for the fields 1 and around 0.9 for the fields 2 and 3, see Fig. 3. Every field reached the maximum biomass production right before harvest and the minimum biomass before harvest was measured in the field 1, see Fig. 3. The slope of the biomass production changes during the crop development and was maximum around the middle of the cycle. A declining tendency appears at the final of the growing cycle coinciding with ripening and maturity stages. This effect has been previously described (Dohleman and Long, 2009) and these authors point to the reduction in plant assimilation because of leaf aging in contrast with the relative high levels of plant respiration.

The analysis of the water stress, see Fig. 3, indicate low levels of water stress in the field 1 and no water stress conditions in the fields 2 and 3. The cold temperature stress was only evident during February and the beginning of March and, in general, these stresses only affected the beginning of the growing cycle. The measurements of NNI indicate that only fields 1 were slightly affected by nitrogen deficit in some measurement locations with minimum NNI values over 0.7. The subsequent applications of fertilizer promote the nitrogen concentration in the plant to comfort levels. The three measurement locations with minimum NNI values lower than 0.9 from the second measurement date were removed from the calibration of the models efficiencies. From the analysis of the stress coefficients estimated for the fields 1, 2 and 3 and

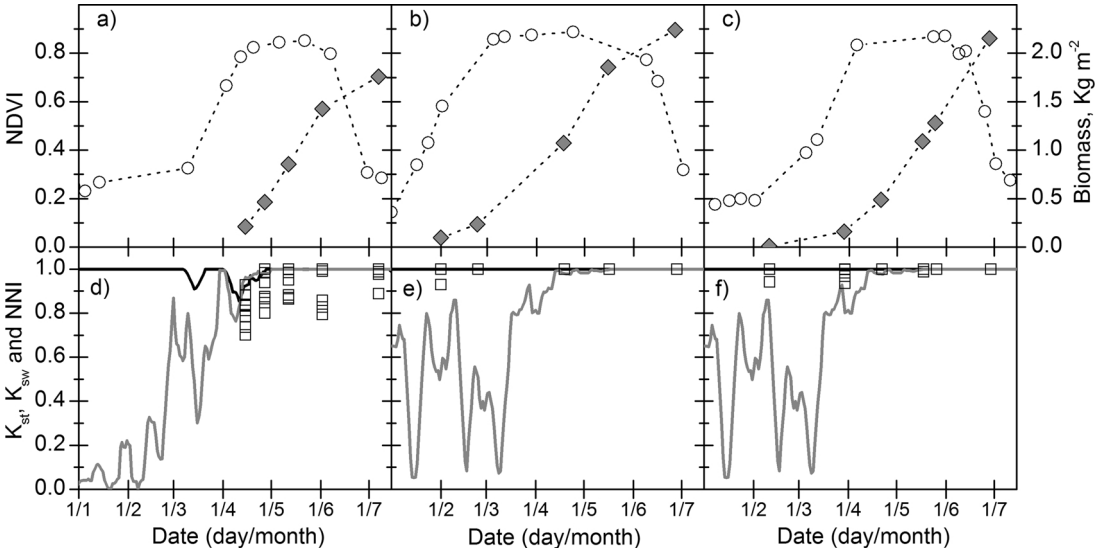

Fig. 3. The upper graphs represent the temporal evolution on the measured NDVI (white circles) and biomass data (grey diamonds) for the calibration datasets for the field 1 (a), field 2 (b) and field 3 (c). The lower graphs represent the temporal evolution of the water stress, (K_{sw} solid black line), the temperature stress (K_{st} grey solid line) and the Nitrogen Nutrition Index, (NNI white squares), for the field 1 (d), field 2 (e) and field 3 (f).

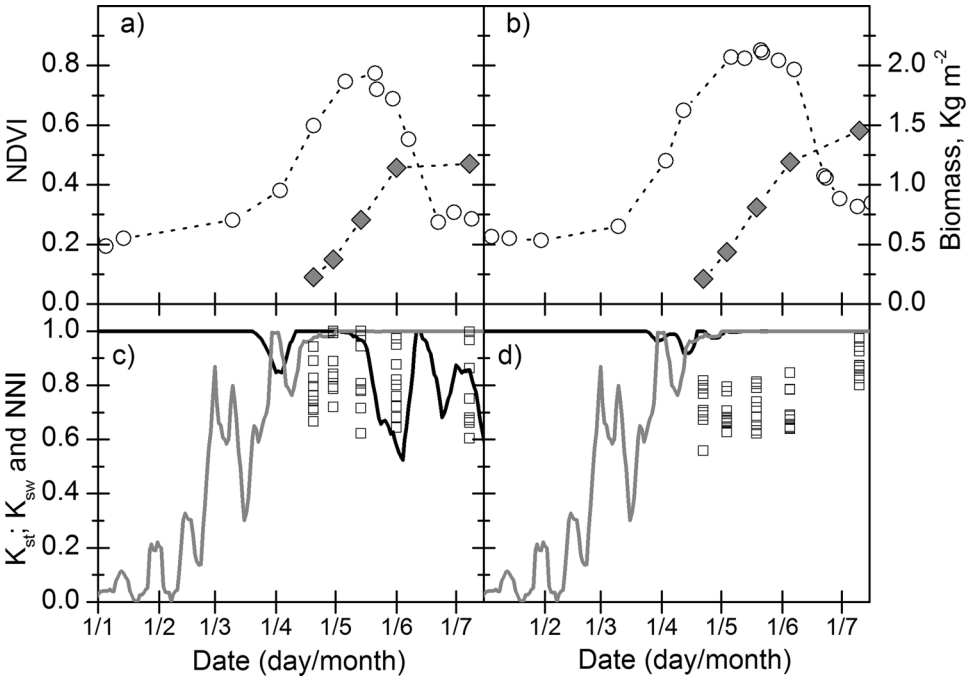

Fig. 4. The upper graphs represent the temporal evolution on the measured NDVI (white circles) and biomass data (grey diamonds) for the field 4 (a) and the field 5 (b) (validation dataset). The lower graphs represent the temporal evolution of the water stress, (K_{sw} solid black line), the temperature stress (K_{st} grey solid line) and the Nitrogen Nutrition Index, (NNI white squares) for the field 4 (c) and the field 5 (d).

the high values of grain yield obtained (see Table 1) we concluded that these fields are in optimum conditions, as needed for the calibration of the efficiency parameters of the models analyzed in this work.

The analysis of the variability indicates that the measurement locations were very homogeneous in the calibration dataset. The SD estimated for the accumulated value of NDVI was lower than the 3% of the mean values in each measurement location. The greater differences was obtained in one measurement locations in the field 3 (SD = 2.26, equivalent to the 2.45% of the mean value). The most homogeneous measurement locations correspond to the field 2, the greatest differences obtained in any location was lower than the 2% of the average value in this field.

3.1.2. Validation dataset

The canopy growth described by the NDVI values in the fields 4 and 5 was similar to those evolutions described for the calibration dataset, see Fig. 4, but the temporal evolution of the NDVI was slightly different for the field 6, Fig. 5. The field 6 was planted with winter wheat and thus the sowing dates correspond to the previous fall in both analyzed seasons. From the emergence, estimated in late-October, the NDVI values show a rapid growth period followed by a period with a relative stability, or even a decrease trend. This period coincides with the minimum air temperatures registered during the season. From December to January the mean temperature was −1.4 °C and 3.1 °C during the first and second seasons analyzed. After this period, the NDVI restarts the increasing trend up to the beginning of the senescence in May. The NDVI values were around 0.5 during the standing period in both analyzed campaigns in the field 6 and the maximum NDVI values (around 0.7) were registered before the beginning of the senescence, see Fig. 5. The lengths of the growing cycles measured in days, GDD and accumulated ETo are presented in Table 1.

The analysis of the soil water balance only indicates moderate levels of water stress in the field 4 and in the field 6 during the 1999–2000 growing season, see Figs. 4 and 5. The water availability for the field 5 and the rainfed wheat growth in the field 6 during the season 1998–1999 was adequate, see Figs. 4 and 5. The cold temperature stress was evident in field 6 during the winter and it limits the normal crop development up to the beginning of April, coinciding with a sudden increase in the slope of the biomass production data, see Fig. 5. No cold temperature stress was observed in fields 4 and 5 during the growing cycle.

The NNI measured for the field 4 was lower than 0.8 during the whole cycle except in 3 measurement locations. The NNI measured in the field 5 was lower than 0.8 during most of the growing cycle and only reached greater values in the last measurement date. The absolute values and the general trend described by the NNI point to the possible effects of nitrogen deficit in the analyzed fields (Justes et al., 1997). The deficit in water and/or nitrogen registered in these fields reduced the crop production in terms of biomass (Fig. 5) and final yield (see Table 1).

The analysis of the variability indicates that the measurement locations were less homogeneous in the fields 4 and 5 in comparison with the calibration dataset. The SD of the accumulated NDVI for each pixel varies between the 5 and the 6% of the average value for some locations in the field 4. The SD estimated for any measurement location was lower than the 5% of the mean values in the field 5.

3.2. Calibration of the WP*, WUE and LUE approaches

For the empirical determination of the LUE, WUE and WP* we correlated the values of measured biomass and the cumulated values of the target variable for each methodology (IPAR, $T_{c,adj}$, $K_{t,adj}$*K_{st}) obtained in the calibration datasets (Fig. 6). The correlation presents a strong linear relationship for every analyzed variable (Table 4). The slopes of the relationships correspond to the empirical values of LUE, WUE and WP* respectively although the values of the interception for the linear regression equations were statistically different from 0 for every model (Table 4). Instead of the possible impact of the interceptions, the linear approaches describe with reasonable precision the relationship between biomass and the used variables for the whole range of the calibration dataset, even forcing the relationships through the origin. The values of LUE, WUE and WP* obtained forcing the relationships through the origin were 1.77 ± 0.02 g MJ^{-1}, 4.40 ± 0.05 g l^{-1} 17.9 ± 0.2 g m^{-1}, and the R^2 values were greater than 0.98 for every relationship.

The results obtained for the calibration dataset reveal the capacity of the proposed approach to estimate biomass production for spring wheat in the study area. Nevertheless, it is fair to say that the methodology proposed and the values of LUE, WUE and WP* must be regarded as empirical values, potentially affected by local conditions, i.e.

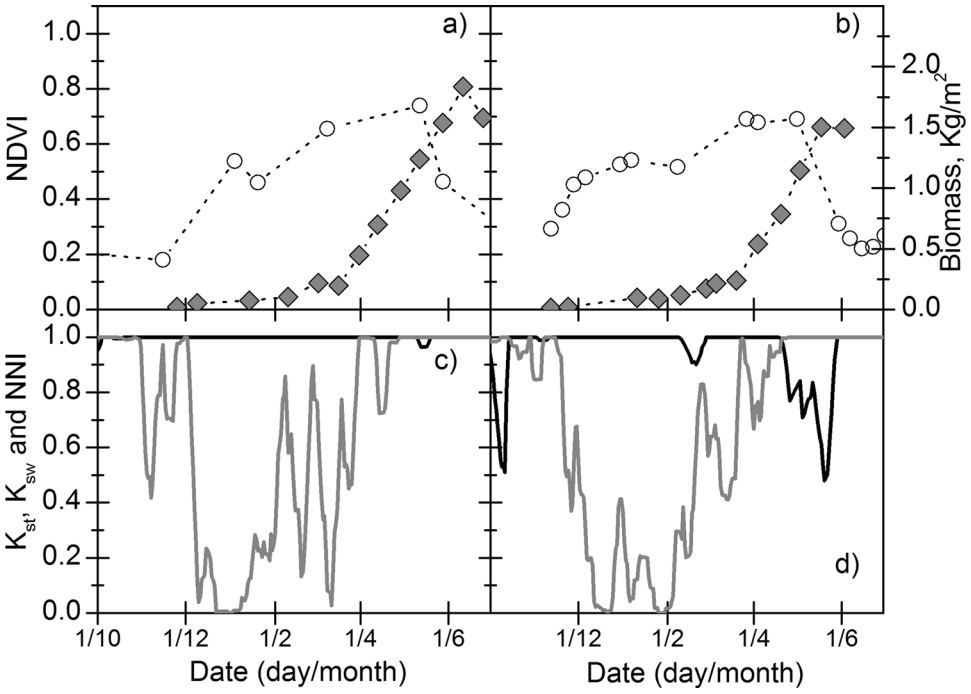

Fig. 5. The upper graphs represent the temporal evolution on the measured NDVI (white circles) and biomass data (white diamonds) for the field 6 (validation dataset) during both analyzed campaigns. The lower graphs represent the temporal evolution of the water stress, (K_{sw} solid black line) and the temperature stress (K_{st} grey solid line).

climate, and other stresses not considered in the analysis. Previous research indicates the factors affecting the empirical values of LUE, WUE and WP* are related with the crop management, mainly water or nitrogen deficits, and the meteorological conditions such as temperature stress and atmospheric demand. These effects were analyzed through the estimation of the biomass production in the validation dataset.

3.3. Models validation

The relationships obtained in this work were applied to the validation dataset with the aim of providing an empirical validation and assuring the reproducibility, and representability of the proposed approaches. In addition, the characteristics of the validation datasets allow to analyze the proposed approach under nitrogen deficit and in two very different climatic conditions (Semiarid Mediterranean and Continental Sub-humid climates). The methodologies were applied to the validations dataset obtained in the fields 4 and 5, subjected to water and nitrogen deficits, and in the field 6 during two consecutive campaigns. The scatter grams of the biomass production measured and simulated by the three approaches indicate a reasonable agreement for every analyzed model, showed in Fig. 7. The best fitting (minimum root mean square error, RMSE, and maximum value of the index of agreement, d) was found for the model based on the product $K_{t,adj}$*K_{st} followed by the model based on $T_{c,adj}$ and the poorest performance was obtained for the model based on IPAR (see Table 5). The greater discrepancies were found at the beginning of the growing cycle, when the measured biomass was lower than 500 g/m^2 for the field 6 and during the ripening physiological stages. While the differences founded at maturity stages did not present a clear pattern, the differences founded for the lower values clearly indicated an overestimation of the models based in IPAR and $T_{c,adj}$. These results are extensively analyzed in the discussion section.

Table 4
Results of the linear regression correlating the biomass measured in the field and the values of accumulated radiation intercepted (IPAR), accumulated basal crop coefficient ($K_{t,adj}$) multiplied by the temperature stress coefficient (K_{st}) and the accumulated product crop transpiration (T_c). The analysis was performed for the whole calibration dataset.

Model	Efficiency	Slope (units)	Interception (units)	R^2
IPAR	LUE	1.88 ± 0.03 (g MJ^{-1})	-88.87 ± 18.48 (g m^{-2})	0.98
$T_{c,adj}$	WUE	4.52 ± 0.09 (g l^{-1})	-38.99 ± 24.85 (g m^{-2})	0.96
$K_{t,adj}$*K_{st}	WP*	20.2 ± 0.3 (g m^{-2})	-187.1 ± 22.8 (g m^{-2})	0.97

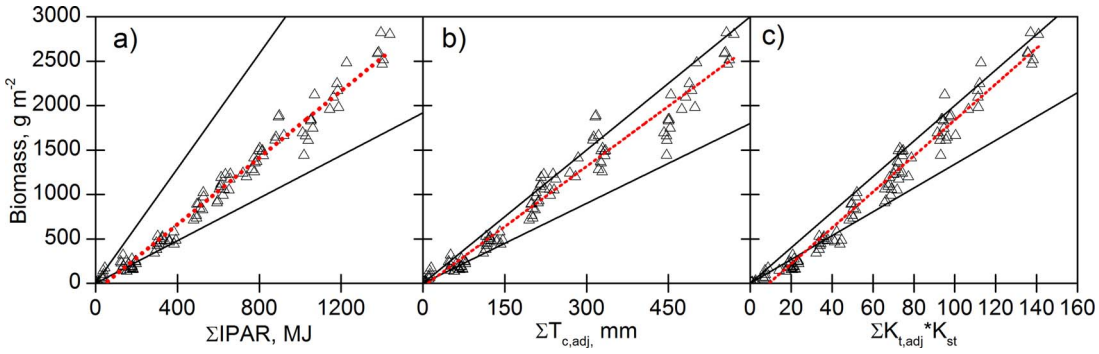

Fig. 6. Correlation between measured biomass and a) the values of accumulated radiation intercepted (IPAR), b) accumulated crop transpiration accounting for water stress ($T_{c,adj}$) and c) the accumulated value of the product of transpiration coefficient accounting for water stress ($K_{t,adj}$) multiplied by the temperature stress coefficient (K_{st}). The dotted line represents the relationships obtained in the model calibration and the solid line represents the range of the efficiencies obtained in the literature review.

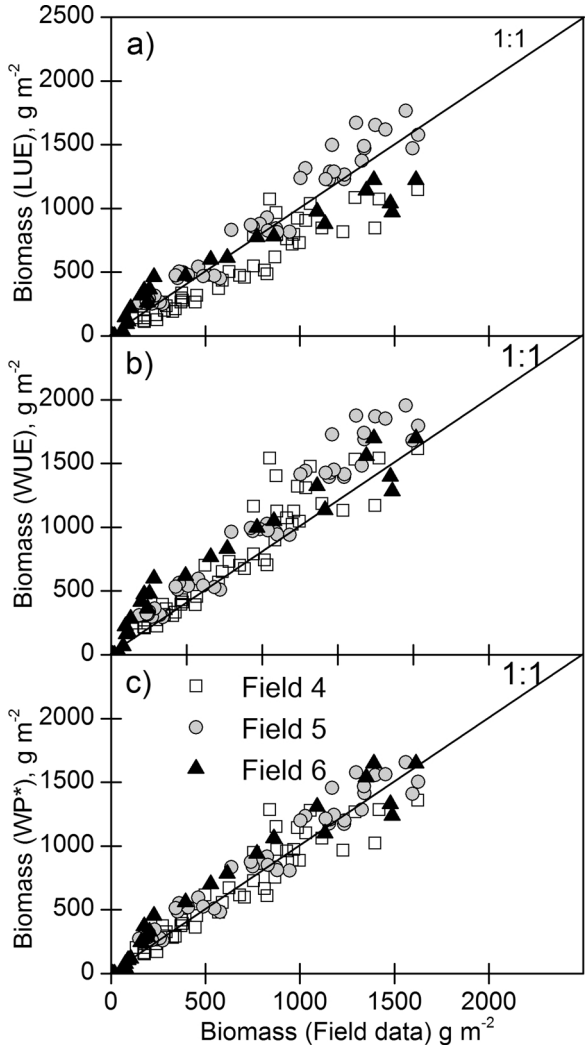

Fig. 7. Comparison of biomass measured in the field and the biomass modeled following the approaches presented in the text: a) accumulated radiation intercepted (IPAR) multiplied by the water stress coefficient, b) accumulated adjusted crop transpiration ($T_{c,adj}$) and c) accumulated adjusted transpiration coefficient ($K_{t,adj}$) multiplied by the temperature stress coefficient (K_{st}).

4. Discussion

4.1. Comparison of the proposed approach and previous developments

The values of the efficiencies obtained in this work were compared with the range of relationships reported in the literature. Only those values obtained for the whole growing cycle and wheat crop managed under non-limiting conditions were considered. Although the literature is scarce in empirical values of WP* for wheat, we found a great collection of empirical values of LUE and WUE for this crop, see Table 6. Our empirical relationship between biomass and the accumulated value of IPAR and the accumulated value of $T_{c,adj}$ coincides with the corresponding mean values of LUE or WUE obtained in the literature review, while the empirical relationship between biomass and the product of $K_{t,adj}$ times K_{st} agree with the higher range of the relationships compiled. The experimental values of the efficiencies founded in this study (LUE, WUE and WP*) were therefore of the right order (correctly adjusted from the calibration dataset). However, it should be noted that the values of LUE obtained for several experiments are not strictly comparable since LUE can be calculated on the basis of absorbed or intercepted radiation, resulting in a difference of about the 5% of the PAR absorption and the consequent propagation of this difference into the LUE values (Gallo and Daughtry, 1986).

The general precision obtained in this work was within the range of other approaches for biomass assessment evaluated in the most recent applications revised. Simulating wheat biomass, Iqbal et al. (2014) obtained a RMSE equal to 87 g/m^2 with the Aquacrop model in experimental plots (5 m × 10 m). Jin et al. (2017a,b) obtained a RMSE over 153 g/m^2 simulating biomass at regional scale (40 samples) using the AQUACROP model calibrated for the area and assimilating remote sensing data (optical and radar). Using the same model calibrated for the study area, Jin et al. (2014) obtained a RMSE equal to 129 g/m^2 simulating the same variable. In view of the results, it is fair to say that the proposed approach does not increase the precision of previous approaches. However, the proposed approaches suppose an operation advantage over crop growth models for the assessment of biomass production at field scale. These advantages can be summarized as follow.

The RS data is a diagnostic of the actual crop development, reflecting the effect of multiple factors that are difficult to consider in the models (i.e. pests and diseases) or are generally unknown working in great areas (i.e. planting dates, varieties, density and emergence rates). On the other hand, RS techniques allow for a quantitative and direct estimation of the core variables related with biomass production, namely fPAR or K_t. A common criticism is that RS techniques are subjected to a high degree of empiricism, and the algorithms can be considered valid for a limited number of crops. But it is fair to say that any estimation of biomass production based on the simulation of crop development requires, at least, two steps that have been validated for a narrow number of crops and contains a similar degree of empiricism as presented in the introductory section. In addition, the proposed approach based on RS data could be useful for the operational assessment of in-field heterogeneity considering the availability of satellite platforms with spatial resolution up to 10 m, although this capability must be analyzed in future works.

The main limitation of the approach proposed is the predictive role recognized to the crop growth models. Nevertheless, the methodology, algorithms and calibration values obtained in this work can be used to evaluate the performance of these models under different climatic conditions and data availability. In addition, it should be noted that the direct integration of the temporal evolution of the needed variables, into the crop growth models compounds a deterministic approach for which the errors in the estimation of the needed variables are

Table 5
Resume of the statistics obtained in the validation of the models based on the intercepted PAR (IPAR), the crop transpiration accounting for water stress ($T_{c,adj}$) and the product of the crop coefficient accounting for water stress ($K_{t,adj}$) by the temperature stress coefficient (K_{st}). The statistics used are the root mean square error (RMSE), the index of agreement (d) and the P-value derived from the two paired samples T-test.

	LUE model			WUE model			WP* model		
	RMSE (g m^{-2})	d (Wilmot)	P (T-test)	RMSE (g m^{-2})	d (Wilmot)	P (T-test)	RMSE (g m^{-2})	d (Wilmot)	P (T-test)
Field 4	203	0.922	0.060	195	0.942	0.270	141	0.964	0.949
Field 5	139	0.978	0.404	251	0.940	0.060	126	0.980	0.466
Field 6 (98–99)	156	0.976	0.793	196	0.972	0.513	158	0.982	0.641
Field 6 (99-00)	218	0.951	0.488	208	0.956	0.489	107	0.990	0.793

Table 6
Empirical values of LUE, WP* and WUE founded in the literature review.

Reference	LUE, g MJ^{-1}	Reference	WUE, g l^{-1}	Reference	WP*, g m^{-2}
Gallagher and Biscoe (1978)	2.2	French and Schultz (1984)	3.7	Steduto and Albrizio (2005)	13.4
Green (1987)	2.0	Siddique et al. (1990)	5.0	Raes et al. (2011) C3 species	15.0–20.0
Garcia et al. (1988)	3.13	Gregory et al. (1992)	3.0	Mkhabela and Bullock (2012)	14.0
Gregory et al. (1992)	1.74	Steduto and Albrizio (2005)	4.5	Iqbal et al. (2014)	15.0
Fischer (1993)	2.58	Sadras and Angus (2006)	4.4		
Calderini et al. (1997)	2.2	Pradhan et al. (2014)	3.2		
Latiri-souki et al. (1998)	2.1				
Lobell et al. (2003)	2.19				
Albrizio and Steduto (2005)	1.7				
Padilla et al. (2012)	2.5				
Pradhan et al. (2014)	2.49				

undoubtedly translated to the model result. This circumstance increases the uncertainty in the determination of the desired variables, and further analysis considering the possible use of assimilation processes are desirable.

4.2. Comparison of the models based on LUE, WUE and WP*

The three approaches were able to reproduce the behavior of the biomass production in the analyzed dataset. The p value for the two samples paired T-test indicate that the mean values were nor statistically different at the 0.05 level (see Table 5). However, the models based on water use were demonstrated more precise in the analyzed environments, being the average RMSE lower for the estimates based on these models (see Table 5). Specifically, the model based on WP* provides the most precise estimation with lower RMSE and higher values of d (see Table 5). In contrast, the correlation between the analyzed variables (APAR, $T_{c,adj}$ and $K_{t,adj}$*K_{st}) indicate the opposite trend. The higher correlation coefficient was obtained for the linear regression between biomass and APAR while the regressions between biomass and $T_{c,adj}$ or $K_{t,adj}$*K_{st} yield lower values for the r^2 (see Table 4). It should be noted that the calibration dataset was obtained under similar meteorological conditions, in the same area although in different growing seasons, and these fields were well managed (no severe stresses). In contrast, the validation dataset was obtained for a wide range of climatic conditions, including frozen periods (Field 6) and some periods of water stress (Field 4). We interpret that the model based on LUE trend to overestimate the biomass production in the Field 4 because the effects of water stress are not considered in this approach (see Fig. 7). The results also indicate that the normalization of the atmospheric conditions in the WP* model could provide a relative advantage with respect to the WUE model as discussed below.

The analysis provided excluded water and nutrient stresses as the main source of variability for some fields. Under these conditions, WUE and LUE models are equivalent and provided similar performance. We consider that this relative good agreement for both models is a novel result and suggests interesting perspectives. The accumulation of biomass increases under conditions of elevated incoming radiation attending to the LUE model, while the accumulation of biomass will be higher in the climates with high atmospheric demand attending to the WUE model. Apparently, both models will diverge when the balance between incoming radiation (PAR) and ETo changes with respect to the climatic conditions analyzed in this study although the extent of this divergence should be analyzed in future works. Further research will be needed to determine the effect of this balance on biomass accumulation, in absence of other abiotic stresses or saturation effects. In particular the analysis of the plasticity of different varieties and the development of indicators of wheat productivity based in the noted balance should be considered.

4.3. Effect of the stresses considered in the models

The effect of water stress in biomass production was not extensively analyzed in this work, because the water deficit was not evident for any field during the entire growing season. However, the poor performance of the LUE model in some of the fields used for validation (Field 4) can be attributed to the effect of the water stress reducing the biomass production over the potential simulated by the model. This circumstance must be analyze in future works and based in more complete datasets, including rainfed fields in semiarid conditions. According with the proposed approach, the effects of water stress can be included by estimating the water stress coefficients. It requires the simulation of the soil water balance or alternative approaches to water stress. Most of the information required for the estimation of water stress is not generally available for great areas, i.e. soil depth, irrigation timing and amounts. However, and even under these conditions (water stressed crops with few information available) the proposed methodology could be interesting. The time integral of T_c, APAR and K_t obtained from reflectance based VIs and meteorological data, appears to be a valuable tool, providing a quantitative indication of potential biomass accumulation and could be used for the assessment of the spatial variability at field scale (Campos et al., 2017a). The effect of the water stress will reduce the actual biomass production, but the extent of this reduction should be analyzed in future works.

While the model based on WP* provides the most precise estimation, the improvement endorsed to WP* was not evident in the validation dataset. The main criticism to the WUE approaches is the dependence of this variable with respect to the atmospheric demand. The normalization of WUE for the climatic conditions in terms of VPD or alternatively ETo was discussed in-depth by Steduto and Albrizio (2005) and Steduto et al. (2007) and summarized by Perry et al. (2009). These authors noted that while the water productivity of a plant is essentially linear for a given situation, the slope of that relationship varies from one place to another and between different seasons, but WUE is extremely stable for a given evaporative demand. So far, the variability of WUE observed between different varieties of the same species is around 10% when WUE is normalized for climatic conditions, equivalent to the concept of WP*. Our results indicate that both approaches, WP* and WUE could be considered equivalent in the noted conditions, for a wide range of climatic data, with a variety of ETo (from 390 to 620 mm of ETo registered during the growing season). Even considering that the statistics indicate a reasonable agreement, the precision of the LUE/WUE model could be improved during the initial phases of crop development, being these effects more evident in the field 6. The noted overestimation can be endorsed to the effects of cold stress, reducing, or even bringing to a standstill, the biomass production. This effect is crop dependent but can be simulated by the cold stress based on growing degree days used in this study, K_{st}.

The biomass production in the locations affected by nitrogen deficit did not differ significantly from the models estimates on these points. In particular, the precision of the models in the field 5, under nitrogen

deficit, was comparable to the precision of the models in other fields. These conclusions are in the line of the relative stability of LUE under nitrogen deficit conditions described by Garcia et al. (1988). These authors demonstrated experimentally that the nitrogen deficit affects mainly the canopy development and thus the ability of the canopy to intercept PAR but the efficiency of the conversion is similar under different applications of nitrogen. Thus, the impact of nitrogen deficit can be considered similar to the water stress, reducing canopy development (Hsiao et al., 2007) and this reduction can be reflected by the spectral measurements. These conclusions are in apparent opposition with other results founded in the literature (Latiri-souki et al., 1998; Lobell et al., 2003; Pradhan et al., 2014). This apparent incongruence is indicating that while the effect of nitrogen deficit reducing the noted efficiencies must be considered, but this effect is unappreciable for the nitrogen contents reported in this study with a range of NNI from 0.6 to greater than 1. The range of NNI obtained in this study is narrower than the ranges obtained in experimental conditions, in which the treatments can be designed to induce high levels of nitrogen deficit. However, the nitrogen concentrations obtained in this study correspond to the deficit levels that can be expected in commercial farms.

4.4. Effects of the satellite time resolution and future improvements

As demonstrated in the literature review, the relationship between NDVI, or alternative multispectral vegetation indices, is a simple and validated method for the estimation of the biophysical parameters used in this work (fPAR and K_t). In addition these simple relationships permits the use of multiple platforms, including the Landsat constellation, as presented in this work, and high resolution images as is the case of Sentinel 2-A and Sentinel 2-B. The compatibility between the images provided by these sensors in terms of surface reflectance and NDVI is analyzed in a recent research (Flood, 2017) and the use of all the available platforms in virtual constellations (Martinez-Beltran et al., 2009) provides an unnoticed temporal resolution using exclusively free and open access images. A preliminary study combining both satellite platforms for the analysis of the spatial variability in biomass production was presented by Campos et al. (2017a).

While additional images sources can be considered, and the combination of multiple platforms is desirable in future works, the time series analyzed in this study were considered enough to describe the evolution of the crop growth using exclusively Landsat images. Within the field campaigns analyzed in this work, the field 6 contains the lower number of images (6 images) due to the scarcity of operational platforms during the years 1998–1999. Nevertheless, the images analyzed are well distributed along the growing season and the inflexion points of the growing curve is well reproduced by the temporal evolution of the NDVI. The precision of the model evaluation quantify as RMSE for the field 6 is within the range obtained for other fields, see Table 5. We want to highly that the number of images must be enough to describe the inflexion points of the growing curve, rather than recommending the minimum number of images necessary for the application of the proposed approach. The evolution of the crop can be assumed linear during the intermediate periods but the availability of images during these periods could also promote the precision of this approach.

5. Conclusions and REMARKS

The analyzed approaches based on the direct estimation of biomass accumulation using RS data, provide good agreement with experimental results for wheat crops grown under very different climatic conditions (Semiarid Mediterranean and Continental Sub-humid climates) and management conditions in commercial fields. The time series of NDVI based on Landsat images describe the crop growth and enable us to estimate the needed parameters, crop transpiration and PAR interception, jointly with meteorological data. The correlation between measured biomass and the key parameter used in each approach exhibits a strong linear correlation for the whole range of calibration data. The slope and bias of these relationships show good agreement with values quantified in other studies.

The basis for all models are well established and the aptitudes have been demonstrated for winter and spring wheat under a variety of climatic conditions. Different conclusions can be obtained for the same crop growing in very extreme climatic conditions or different crops growing in different seasons as is the case of winter and spring crops versus summer crops. In addition, the stability of these results under middle/moderate stress, either temperature and nitrogen origin, seems to support the proposed methodology to estimate biomass accumulation. The reasons behind this behavior could be the capability of the RS data (NDVI values) to reflect the effect of the noted stresses reducing the canopy development. Nevertheless, further research will be needed to establish the limits of these approaches under severe stress conditions that lead to closing stoma. Hence, time integral, that is the area under the curve of T, APAR or K_t estimated using the satellite reflectance based VIs and meteorological data, is a valuable tool for biomass monitoring in absence of stresses or under low levels of nitrogen deficit. These simple approaches provide a quantitative indication of potential biomass accumulation because the noted stresses only could decrease the accumulation rate.

Finally, the results obtained in this work opens the possibility for further interesting applications as is the characterization of field homogeneity and further advances for the estimation of crop yield based on RS data, considering that the potential harvestable yield determined from RS data described the upper limit of yield assuming non-limiting conditions for the remainder of the growth cycle. Other interesting applications will be the combination of the proposed methodology for biomass estimation and the use of RS methods to estimate nitrogen concentration.

Acknowledgements.

This research was developed in the framework of the projects HERMANA (HERramientas para el MAnejo sostenible de fertilización Nitrogenada y Agua), funded by the Spanish Ministry Science and Innovation (AGL2015-68700-R) and FATIMA (FArming Tools for external nutrient Inputs and water MAnagement), funded by the < gs3 > European Unionś Horizon 2020 research and innovation programme < /gs > (Grant Agreement No 633945). The authors of this paper are the researchers that collaborate actively analyzing the data and preparing the manuscript, but we must acknowledge the effort of the persons involved in the data collection and processing in the fields located in Albacete (M. Calera and N. Jimenez from ALIARA AGRICOLA s.l., J. Campoy and C. Plaza from AGRISAT s.l., S. Sánchez and E. Sánchez from IDR-UCLM and F.M. Jara, I. Narro, F. Alonso, B. Quirós, H. Alcaraz, E. Pareja and P. Avilés from Instituto Técnico Agronómico Provincial). The satellite images were downloaded from the Surface Reflectance Climate Data Record (CDR) of the USGS (http://landsat.usgs.gov/CDR_LSR.php). The ground data for Ponca site were downloaded from the Ameriflux database (http://ameriflux.ornl.gov/).

References

Aase, J.K., Siddoway, F.H., 1981. Assessing winter wheat dry matter production via spectral reflectance measurements. Remote Sens. Environ. 11, 267–277.
Albrizio, R., Steduto, P., 2005. Resource use efficiency of fieldgrown sunflower, sorghum, wheat and chickpea. I. Radiation use efficiency. Agric. For. Meteorol 130, 254–268.
Allen, R.G., Raes, D., Smith, M., 1998. Crop Evapotranspiration: Guidelines for Computing Crop Requirements. Irrig. Drain. Pap. No. 56, FAO, Rome, Italy.
Angus, J., Moncur, M., 1985. Models of growth and development of wheat in relation to plant nitrogen. Aust. J. Agric. Res. 36, 537–544.
Asrar, G., Fuchs, M., Kanemasu, E.T., Hatfield, J.L., 1984. Estimating absorbed photosynthetic radiation and leaf area index from spectral reflectance in wheat. Agron. J. 76, 300–306.
Baret, F., Guyot, G., 1991. Potentials and limits of vegetation indices for LAI and APAR assessment. Remote Sens. Environ. 35, 161–173.
Bastiaanssen, W.G.M., Ali, S., 2003. A new crop yield forecasting model based on satellite

measurements applied across the Indus Basin, Pakistan. Agric. Ecosyst. Environ. 94, 321–340.
Bausch, W.C., Neale, C.M.U., 1987. Crop coefficients derived from reflected canopy radiation – a concept. Trans. ASAE 30, 703–709.
Bouman, B.A.M., 1992. Linking physical remote sensing models with crop growth simulation models, applied for sugar beet. Int. J. Remote Sens. 13, 2565–2581.
Briggs, L.J., Shantz, H.L., 1913. The Water Requirement of Plants. I. Investigations in the Great Plains in 1910 and 1911. U.S. Dept. Agric. Bur. Plant Ind. Bull, pp. 1–48.
Brisson, N., Mary, B., Ripoche, D., Jeuffroy, M.H., Ruget, F., Nicoullaud, B., Gate, P., Devienne-Barret, F., Antonioletti, R., Durr, C., Richard, G., Beaudoin, N., Recous, S., Tayot, X., Plenet, D., Cellier, P., Machet, J.-M., Meynard, J.M., Delécolle, R., 1998. STICS: a generic model for the simulation of crops and their water and nitrogen balances. I. Theory and parameterization applied to wheat and corn. Agronomie 18, 311–346.
Burba, G., Verma, S.B., 2005. Seasonal and interannual variability in evapotranspiration of native tallgrass prairie and cultivated wheat ecosystems. Agric. Forest Meteorol. 135, 190–201.
Calderini, D.F., Dreccer, M.F., Slafer, G.A., 1997. Consequences of breeding on biomass, radiation interception and radiation-use efficiency in wheat. F. Crop. Res. 52, 271–281.
Calera, A., González-Piqueras, J., Melia, J., 2004. Monitoring barley and corn growth from remote sensing data at field scale. Int. J. Remote Sens. 25, 97–109.
Campbell, G.S., Norman, J.M., 1998. An Introduction to Environmental Biophysics, 2nd ed. .
Campos, I., Neale, C.M.U., López, M.L., Balbontin, C., Calera, A., 2014. Analyzing the effect of shadow on the relationship between ground cover and vegetation indices by using spectral mixture and radiative transfer models. J. Appl. Remote Sens. 8, 83562.
Campos, I., Balbontin, C., González-Piqueras, J., González-Dugo, M.P., Neale, C., Calera, A., 2016. Combining water balance model with evapotranspiration measurements to estimate total available water soil water in irrigated and rain-fed vineyards. Agric. Water Manag. 165, 141–152.
Campos, I., González, L., Villodre, J., Calera, M., Campoy, J., Jiménez, N., Plaza, C., Calera, A., 2017a. Mapping within-field biomass variability: a remote sensing-based approach. Adv. Anim. Biosci. 8, 764–769.
Campos, I., Neale, C.M.U., Arkebauer, T., Suyker, A., Gonçalves, I., 2017b. Water productivity and crop yield: a simplified remote sensing driven operational approach. Agric. For. Meteorol. http://dx.doi.org/10.1016/j.agrformet.2017.07.018.
Campos, I., Neale, C.M.U., Suyker, A., Arkebauer, T., Gonçalves, I., 2017c. Reflectance-based crop coefficients REDUX: for operational evapotranspiration estimates in the age of high producing hybrid varieties. Agric. Water Manag. 187, 140–153.
Chen, X., Vierling, L., Deering, D., 2005. A simple and effective radiometric correction method to improve landscape change detection across sensors and across time. Remote Sens. Environ. 98, 63–79.
Choudhury, B.J., Ahmed, N.U., Idso, S.B., Reginato, R.J., Daughtry, C.S., 1994. Relations between evaporation coefficients and vegetation indices studied by model simulations. Remote Sens. Environ. 50, 1–17.
Clevers, J.G.P.W., Büker, C., van Leeuwen, H.J.C., Bouman, B.A.M., 1994. A framework for monitoring crop growth by combining directional and spectral remote sensing information. Remote Sens. Environ. 50, 161–170.
Daughtry, C.S.T., Gallo, K.P., Goward, S.N., Prince, S.D., Kustas, W.P., 1992. Spectral estimates of absorbed radiation and phytomass production in corn and soybean canopies. Remote Sens. Environ. 39, 141–152.
Dohleman, F.G., Long, S.P., 2009. More productive than maize in the midwest: how does miscanthus do it? Plant Physiol. 150, 2104–2115.
Duchemin, B., Hadria, R., Er-Raki, S., Boulet, G., Maisongrande, P., Chehbouni, A., Escadafal, R., Ezzahar, J., Hoedjes, J.C.B., Kharrou, M.H., Khabba, S., Mougenot, B., Olioso, A., Rodriguez, J.C., Simmoneaux, V., 2006. Monitoring wheat phenology and irrigation in central Morocco On the use of relationships between evapotranspiration, crop coefficients, leaf area index and remotely-sensed vegetation indices. Agric. Water Manag. 79, 1–27.
Er-Raki, S., Chehbouni, A., Guemouria, N., Duchemin, B., Ezzahar, J., Hadria, R., 2007. Combining FAO-56 model and ground-based remote sensing to estimate water consumptions of wheat crops in a semi-arid region. Agric. Water Manag. 87, 41–54.
Fischer, R., Maurer, R., 1978. Drought resistance in spring wheat cultivars. I. Grain yield responses. Aust. J. Agric. Res. 29 (5), 897.
Fischer, R.A., 1993. Irrigated spring wheat and timing and amount of nitrogen fertilizer. II. Physiology of grain yield response. Field. Crop Res. 33, 57–80.
Fitzgerald, G.J., Rodriguez, D., Christensen, L.K., Belford, R., Sadras, V.O., Clarke, T.R., 2006. Spectral and thermal sensing for nitrogen and water status in rainfed and irrigated wheat environments. Precis. Agric. 7, 233–248.
Flood, N., 2017. Comparing sentinel-2A and landsat 7 and 8 using surface reflectance over Australia. Remote Sens. 9. http://dx.doi.org/10.3390/rs9070659.
French, R., Schultz, J., 1984. Water use efficiency of wheat in a Mediterranean-type environment. I. The relation between yield, water use and climate. Aust. J. Agric. Res. 35, 743.
Gallagher, J.N., Biscoe, P.V., 1978. Radiation absorption, growth and yield of cereals. J. Agric. Sci. 91, 47–60.
Gallo, K., Daughtry, C., 1986. Techniques for measuring intercepted and absorbed photosynthetically active radiation in corn canopies. Agron. J. 78 (4), 752–756.
Garcia, R., Kanemasu, E.T., Blad, B.L., Bauer, A., Hatfield, J.L., Major, D.J., Reginato, R.J., Hubbard, K.G., 1988. Interception and use efficiency of light in winter wheat under different nitrogen regimes. Agric. For. Meteorol. 44, 175–186.
Glenn, E.P., Huete, A.R., Nagler, P.L., Nelson, S.G., 2008. Relationship between remotely-sensed vegetation indices, canopy attributes and plant physiological processes: what vegetation indices can and cannot tell us about the landscape. Sensors 8 (4), 2136–2160.
Glenn, E.P., Neale, C.M.U., Hunsaker, D.J., Nagler, P.L., 2011. Vegetation index-based crop coefficients to estimate evapotranspiration by remote sensing in agricultural and natural ecosystems. Hydrol. Process. 25, 4050–4062.
González, L., Campos, I., Calera, A., 2017. Desempeño de las métricas temporales número de días, grados-día y evapotranspiración de referencia. In: XVII Congreso de La Asociación Española de Teledetección. Murcia, Spain.
González-Dugo, M.P., Mateos, L., 2008. Spectral vegetation indices for benchmarking water productivity of irrigated cotton and sugarbeet crops. Agric. Water Manag. 95, 48–58.
Gonzalez-Dugo, M.P., Neale, C.M.U., Mateos, L., Kustas, W.P., Prueger, J.H., Anderson, M.C., Li, F., 2009. A comparison of operational remote sensing-based models for estimating crop evapotranspiration. Agric. For. Meteorol. 149, 1843–1853.
Green, C.F., 1987. Nitrogen nutrition and wheat growth in relation to absorbed solar radiation. Agric. For. Meteorol. 41, 207–248.
Greenwood, D., Neeteson, J., Draycott, A., 1986. Quantitative relationships for the dependence of growth rate of arable crops on their nitrogen content, dry weight and aerial environment. Plant Soil 91, 281–301.
Gregory, P., Tennant, D., Belford, R., 1992. Root and shoot growth, and water and light use efficiency of barley and wheat crops grown on a shallow duplex soil in a mediterranean-type environment. Aust. J. Agric. Res. 43, 555.
Hoogenboom, G., 2000. Contribution of agrometeorology to the simulation of crop production and its applications. Agric. For. Meteorol. 103, 137–157.
Houlès, V., Guérif, M., Mary, B., 2007. Elaboration of a nitrogen nutrition indicator for winter wheat based on leaf area index and chlorophyll content for making nitrogen recommendations. Eur. J. Agron. 27, 1–11.
Hsiao, T.C., Steduto, P., Fereres, E., 2007. A systematic and quantitative approach to improve water use efficiency in agriculture. Irrig. Sci. 25, 209–231.
Hunsaker, D.J., Pinter, P.J., Barnes, E.M., Kimball, B.A., 2003. Estimating cotton evapotranspiration crop coefficients with a multispectral vegetation index. Irrig. Sci. 22, 95–104.
Iqbal, M.A., Shen, Y., Stricevic, R., Pei, H., Sun, H., Amiri, E., Penas, A., del Rio, S., 2014. Evaluation of the FAO AquaCrop model for winter wheat on the North China Plain under deficit irrigation from field experiment to regional yield simulation. Agric. Water Manag. 135, 61–72.
Jin, X.L., Feng, H.K., Zhu, X.K., Li, Z.H., Song, S.N., Song, X.Y., et al., 2014. Assessment of the AquaCrop model for use in simulation of irrigated winter wheat canopy cover, biomass, and grain yield in the North China plain. PLoS One 9 (1). http://dx.doi.org/10.1371/journal.pone.0086938.
Jin, X., Li, Z., Yang, G., Yang, H., Feng, H., Xu, X., Wang, J., Li, X., Luo, J., 2017a. Winter wheat yield estimation based on multi-source medium resolution optical and radar imaging data and the AquaCrop model using the particle swarm optimization algorithm. ISPRS J. Photogramm. Remote Sens. 126, 24–37.
Jin, X., Li, Z., Yang, G., Yang, H., Feng, H., Xu, X., et al., 2017b. Winter wheat yield estimation based on multi-source medium resolution optical and radar imaging data and the AquaCrop model using the particle swarm optimization algorithm. ISPRS J. Photogramm. Remote Sens. 126, 24–37.
Jones, C.A., Kiniry, J.R., 1986. CERES-Maize: A Simulation Model of Maize Growth and Development. Texas A&M University Press, College Station, Tx.
Jones, J.W., Hoogenboom, G., Porter, C.H., Boote, K.J., Batchelor, W.D., Hunt, L.A., Wilkens, P.W., Singh, U., Gijsman, A.J., Ritchie, J.T., 2003. The DSSAT cropping system model. Eur. J. Agron. 18, 235–265.
Justes, E., Jeuffroy, M., Mary, B., 1997. Wheat, barley and durum wheat. In: Lemaire, G. (Ed.), Diagnosis of the Nitrogen Status in Crops. Springer-Verlag, Berlin Heidelberg, pp. 73–91.
Latiri-souki, K., Nortcliff, S., Lawlor, D.W., 1998. Nitrogen fertilizer can increase dry matter, grain production and radiation and water use e Y ciencies for durum wheat under semi-arid conditions. Eur. J. Agron. 9, 21–34.
Lobell, D.B., Asner, G.P., Ortiz-Monasterio, J.I., Benning, T.L., 2003. Remote sensing of regional crop production in the Yaqui Valley, Mexico: estimates and uncertainties. Agric. Ecosyst. Environ. 94, 205–220.
Lobell, D.B., Ortiz-Monasterio, J.I., Sibley, A.M., Sohu, V.S., 2013. Satellite detection of earlier wheat sowing in India and implications for yield trends. Agric. Syst. 115, 137–143.
Marshall, M., Thenkabail, P., Biggs, T., Post, K., 2016. Hyperspectral narrowband and multispectral broadband indices for remote sensing of crop evapotranspiration and its components (transpiration and soil evaporation). Agric. For. Meteorol. 218 (-219), 122–134.
Martinez-Beltran, C., Jochum, M.A.O., Calera, A., Melia, J., 2009. Multisensor comparison of NDVI for a semi-arid environment in Spain. Int. J. Remote Sens. 30, 1355–1384.
McMaster, G.S., Smika, D.E., 1988. Estimation and evaluation of winter wheat phenology in the central Great Plains. Agric. For. Meteorol. 43, 1–18.
Mkhabela, M.S., Bullock, P.R., 2012. Performance of the FAO AquaCrop model for wheat grain yield and soil moisture simulation in Western Canada. Agric. Water Manag. 110, 16–24.
Monteith, J.L., 1972. Solar radiation and productivity in tropical ecosystems. J. Appl. Ecol. 9, 747–766.
Neale, C., Bausch, W., Heerman, D., 1989. Development of reflectance-based crop coefficients for corn. Trans. ASAE 32, 1891–1899.
Odi-Lara, M., Campos, I., Neale, C.M.U., Ortega-Farias, S., Poblete-Echeverria, C., Balbontin, C., Calera, A., 2016. Estimating evapotranspiration of an apple orchard using a remote sensing-based soil water balance. Remote Sens. 8. http://dx.doi.org/10.3390/rs8030253.
Padilla, F.L.M., Maas, S.J., González-Dugo, M.P., Mansilla, F., Rajan, N., Gavilán, P., Domínguez, J., 2012. Monitoring regional wheat yield in Southern Spain using the GRAMI model and satellite imagery. F. Crop. Res. 130, 145–154.

Perry, C., Steduto, P., Allen, R.G., Burt, C.M., 2009. Increasing productivity in irrigated agriculture: agronomic constraints and hydrological realities. Agric. Water Manag. 96, 1517–1524.
Pinter, P.J.J., Hatfield, J.L.L., Schepers, J.S.S., Barnes, E.M.M., Moran, M.S.S., Daughtry, C.S.T.S.T., Upchurch, D.R.R., 2003. Remote sensing for crop management. Photogramm. Eng. Remote Sens. 69, 647–664.
Pradhan, S., Sehgal, V.K., Sahoo, R.N., Bandyopadhyay, K.K., Singh, R., 2014. Yield, water, radiation and nitrogen use efficiencies of wheat (Triticum aestivum) as influenced by nitrogen levels in a semi-arid environment. Indian J. Agron. 59, 267–275.
Raes, D., Steduto, P., Hsiao, T.C., Fereres, E., 2008. AquaCrop—the FAO crop model to simulate yield response to water: II. Main algorithms and software description. Agron. J. 101, 438–447.
Raes, D., Steduto, P., Hsiao, T., Fereres, E., 2011. Aquacrop Reference Manual. FAO, Land and Water Division, Rome, Italy.
Rosenberg, N.J., Blad, B.L., Verma, S.B., 1983. Microclimate: The Biological Environment, 2nd ed. 2nd Wiley, New York.
Sadras, V., Angus, J.F., 2006. Benchmarking water-use efficiency of rainfed wheat in dry environments. Aust. J. Agric. Res. 57, 847–856.
Sadras, V., Cassman, K., Grassini, P., Hall, A., Bastiaanssen, W., Laborte, A., Milne, A., Sileshi, G., Steduto, P., 2015. Yield Gap Analysis of Rainfed and Irrigated Crops: Methods and Case Studies. FAO water reports 41, Rome, Italy.
Sellers, P.J., Berry, J.A., Collatz, G.J., Field, C.B., Hall, F.G., 1992. Canopy reflectance, photosynthesis, and transpiration. III. A reanalysis using improved leaf models and a new canopy integration scheme. Remote Sens. Environ. 42, 187–216.
Sellers, P.J., 1985. Canopy reflectance, photosynthesis and transpiration. Int. J. Remote Sens. 6, 1335–1372.
Sibley, A.M., Grassini, P., Thomas, N.E., Cassman, K.G., Lobell, D.B., 2014. Testing remote sensing approaches for assessing yield variability among maize fields. Agron. J. 106, 24–32.
Siddique, K., Tennant, D., Perry, M., Belford, R., 1990. Water use and water use efficiency of old and modern wheat cultivars in a Mediterranean-type environment. Aust. J. Agric. Res. 41, 431.
Steduto, P., Albrizio, R., 2005. Resource use efficiency of field-grown sunflower, sorghum, wheat and chickpea II: water use efficiency and comparison with radiation use efficiency. Agric. For. Meteorol. 130, 269–281.
Steduto, P., Hsiao, T.C., Fereres, E., 2007. On the conservative behavior of biomass water productivity. Irrig. Sci. 25, 189–207.
Steduto, P., Raes, D., Hsiao, T.C., Fereres, E., Heng, L.K., Howell, T.A., et al., 2009. Concepts and Applications of AquaCrop: The FAO Crop Water Productivity Model. In: Cao, W., White, J.W., Wang, E. (Eds.), Crop Modeling and Decision Support. Springer, Heidelberg, Berlin, pp. 175–191. http://dx.doi.org/10.1007/978-3-642-01132-0_1.
Steduto, P., Hsiao, T.C., Fereres, E., Raes, D., 2012. Crop Yield Response to Water. FAO Irrig. Drain. Pap. No.66 505.
Stockle, C.O., Martin, S., Campbell, G.S., 1994. CropSyst, a cropping systems model: water/nitrogen budgets and crop yield. Agric. Syst. 46, 335–359.
Trombetta, A., Iacobellis, V., Tarantino, E., Gentile, F., 2016. Calibration of the AquaCrop model for winter wheat using MODIS LAI images. Agric. Water Manag. 164, 304–316.
Williams, J.R., Jones, C.A., Dyke, P.T., 1990. The EPIC model. In: Sharpley, A.N., Williams, J.R. (Eds.), EPIC-Erosion/Productivity Impact Calculator: 1. Model Documentation. U.S. Department of Agriculture. Technical Bulletin No. 1768 (p. 235).
Zheng, Y., Zhang, M., Zhang, X., Zeng, H., Wu, B., 2016. Mapping winter wheat biomass and yield using time series data blended from PROBA-V 100- and 300-m S1 products. Remote Sens. 8. http://dx.doi.org/10.3390/rs8100824.
Zwart, S.J., Bastiaanssen, W.G.M., 2007. SEBAL for detecting spatial variation of water productivity and scope for improvement in eight irrigated wheat systems. Agric. Water Manag. 89, 287–296.